ARMA 20-1864

Wellbore Stability and Predicted Cuttings Volume in Deviated Wellbores and Bedded Formations

Tsopela A., Bere A., Dutko M. and Kato J.

Rockfield Software Ltd., Ethos, Kings Road, Prince of Wales Dock, Swansea Waterfront, SA1 8AS, UK

ABSTRACT: The success of hydrocarbon recovery from the subsurface relies on wellbore stability usually provided by suitable mud-weight. Too low can cause breakout and wellbore collapse; too high can cause fractures (breakdown), and thereby giving rise to an operating mud-weight window (MWW). The MWW forms part of the operator's well planning process and is sensitive to in-situ stress estimates, well trajectory and formation material properties. Analytical calculations can estimate the onset of damage around a wellbore; however, this has two inherent limitations in not being able to capture 1) complex stress distribution around wellbores deviated from the in-situ stress direction and/or in non-homogeneous formations, and 2) material softening/hardening due to formation damage and redistribution of stress influencing further damage or stability/instability. 3-dimensional numerical modelling has the capability of capturing stress conditions around wellbores of any orientation, while additionally considering constitutive material models that can capture both heterogeneous characteristics (including bedding plane effects) and post-yield strength softening/hardening. Therefore, with efficient modelling techniques it is possible to capture detailed wellbore stability due to a range of well trajectories and formation anisotropy. By careful consideration of the results it is possible to provide beneficial information for drilling, such as predicted cuttings volume and safe MWW. Such modelling and result assessment techniques are available in the Elfen wellbore software; paper provides detailed assessment of both wellbore deviation and formation heterogeneity with an aim to enhancing current wellbore stability assessments.

1. INTRODUCTION

Similar to mining and tunnelling industries, the oil and gas industry has long acknowledged that instability of subsurface excavations can pose serious problems affecting the timing, risk management and economics of a project. With the oil and gas industry exploring reservoirs under increasingly difficult geological conditions and with complex recovery techniques becoming standard, wellbore stability analysis needs to reflect these challenging environments and account for difficult geological conditions, such as drilling in depleted formations, highly deviated wells or laminated formations. Challenging conditions can also be encountered in other applications dealing with subsurface integrity issues and "reservoir containment geomechanics" (Schultz et al., 2016) such as geothermal fields (Moeck and Bakers, 2011; Ghassemi, 2012) and carbon dioxide sequestration (Streit and Hillis, 2004; Rutqvist, 2012; Zoback and Gorelick, 2012; Altman et al., 2014).

The availability of methods for real-time wellbore imaging, caving monitoring and managed wellbore pressure combined with real-time wellbore stability prediction can provide a robust tool for the planning and management of wells under difficult conditions (Willson et al., 2007). Pre-drill and real-time wellbore stability prediction consists of predicting any possible instability around the wellbore and is principally based on the stress concentration around the wellbore versus the formation strength. Depending on the mud weight, wellbore instability can result in lost circulation, breakouts or hole closure and even in loss of the open-hole section due to stuck and damaged drill pipe (Lang et al., 2011).

Conventional pre-drill wellbore stability analysis considers the linear elastic or poroelastic response of the rock and has been well documented in published literature (e.g. Zoback 2007). Wellbore collapse is expected to occur at a point surrounding the wellbore whenever the elastic/poroelastic stress satisfies the failure criterion of the rock. Although failure criteria, such as Mohr-Coulomb or Drucker-Prager, can inform the onset of plastic yielding, these analyses are usually conservative in predicting the mud weight window (Chen and Abousleiman, 2017). For a more appropriate representation of the formation response and hence a better determination of the minimum mud weight, advanced elastoplastic constitutive models which take

into account the nonlinear hardening or softening behaviour of the rock are necessary.

Due to their depositional history, many sedimentary rocks are characterised by laminated structures, most commonly bedding planes. Numerous experimental studies have shown that such formations exhibit anisotropy in stiffness and strength (e.g. Bonnelye et al., 2017). In the case of extended reach wells, bedding-related wellbore instability can become a significant drilling obstacle; common considerations of homogeneous rock may fail to describe failure under these conditions (Ong and Roegiers, 1993). In-situ observations and experimental results (Willson et al., 1999; Ask and Ask, 2007; Lang et al., 2011; Tellez et al., 2012; Labiouse and Vietor, 2014; Konstantinovskaya et al., 2016; Mehrabian et al., 2018) have shown that, in the presence of bedding planes yielding occurs at the corners of the wellbore unlike the conventional breakouts, and the dominant mechanism is buckling of the exposed bedding leading to subsequent fracturing at the maximum curvature (Okland and Cook, 1998).

While there exists some semi-analytical solutions considering both strain hardening/softening response (Chen et al., 2012; Gaede et al., 2013; Chen and Abousleiman, 2017) and planes of weakness (Zhang, 2013; Zhou et al., 2018), these are usually limited to specific types of rock, well orientations or stress conditions. In addition, there are several numerical models dealing with wellbore stability under complex conditions, however only a few of them are able to accurately account for the post-yield redistribution of stress around the wellbore and capture further potential damage or stability. Efficient numerical modelling used for wellbore stability analysis can capture the mechanism, location and extent of plastic yielding around the wellbore in a range of well trajectories and formation heterogeneities. Consideration of the results provides beneficial information for drilling, such as operating mud weight window and predicted cuttings volume; these can be provided post-yield based on the continuous calculation of the dynamically changing stresses around the wellbore. Such modelling and result assessment techniques are available in the Elfen wellbore software. In the following study, Elfen wellbore software is used to assess wellbore stability in both deviated wells and heterogeneous formations providing insight into the different instability mechanisms and estimates of operational parameters with an emphasis on cuttings volume prediction making use of the software modelling capabilities. Firstly, a vertical wellbore is considered under different stress and pressure conditions reproducing theoretical rupture modes proposed by Etchecopar et al. (1999). Rock heterogeneity is then considered by introducing planes of weakness in the model. Lastly, the wellbore trajectory is modified to estimate the effect of wellbore inclination and angle of attack on the deviated wellbore stability.

2. MODEL SET-UP

Elfen wellbore software is used for the set-up of the model and the numerical simulations. The purpose of the wellbore model is to reproduce rupture modes around the wellbore given different stress conditions and mud weight magnitudes, and to explore the effects of varying formation strength and well orientation. The model used in this study is three-dimensional (3D) and is based on the model presented in Willson et al. (2007).

2.1. Model Geometry

The model consists of a 9.5 inches diameter wellbore, 50 inches long with the boundaries of the domain extending to 95 inches (10×well diameter). As a reference case, the wellbore is considered vertical and aligned with the principal stress directions.

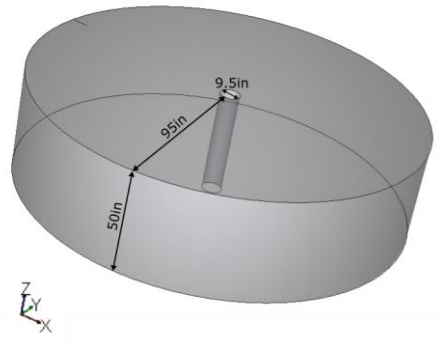

Fig. 1. Model geometry.

The well may be inclined in order to assess the effect of a deviated well and the angle of attack with respect to the in-situ stresses and/or orientation of the planes of weakness; for this paper the well azimuth for inclined case is in the direction of maximum horizontal stress. Well inclinations and bedding orientation are shown in Fig. 2, note the in-situ stresses are maintained as parallel and perpendicular to the bedding in all cases. The angles mentioned in Fig. 2 correspond to the angles of attack between the well axis and the planes of weakness.

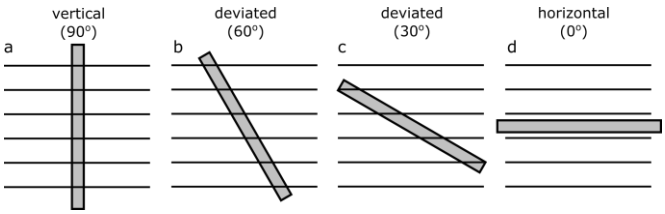

Fig. 2. Well inclination with respect to planes of weakness orientation. The corresponding angles of attack are (a) 90˚, (b) 60˚, (c) 30˚ and (d) 0˚.

2.2. Material Properties

The material properties used in the model represent a sandstone including ±10% stochastically varying elasticity and strength defined by Mohr-Coulomb elasto-plasticity and a Rankine tension cut-off. To capture the post-yield response of the material, strain softening is also accounted for by gradual degradation of the cohesion, friction angle and dilation angle as a function of the plastic strain.

To estimate the effect of strength heterogeneity on wellbore response, planes of weakness (PoW) are included in some of the analyses presented in this study. The PoW properties are represented by 1) elasticity factors normal and tangential to the planes of weakness which are defined as a factor of the host rock Young's and shear moduli, and 2) the plastic properties in terms of cohesion and friction angle are in the range of values used in the study from Zhang (2013). The properties of the planes of weakness together with the host rock properties are summarised in Table 1, it should be noted that the tensile strength across PoW is considered zero.

Table 1. Host rock properties

Host Rock Elastic Properties	
Young's Modulus, E (psi)	3e6
Poisson's Ratio, ν (-)	0.2
Density, ρ (g/cc)	0.0058
Host Rock Plastic Properties	
Cohesion, c (psi)	865
Friction Angle, ϕ (°)	30
Dilatancy, ψ, (°)	30
Uniaxial Compressive Strength, *UCS* (psi)	2995
Tensile Strength, σ_t (psi)	217
Planes of Weakness Elastic Properties	
Stiffness Ratio Normal to PoW, E_w/E (-)	0.5
Stiffness Ratio Tangential to PoW, G_w/G (-)	0.5
Cohesion, c_w (psi)	200
Friction Angle, ϕ_w (°)	15
Tensile Strength, σ_t (psi)	0

2.3. *Initial Conditions*

In order to reproduce the basic rupture patterns a vertical well, aligned with a principal stress is considered. According to Etchecopar et al. (1999), under compressional stress states there are six theoretical rupture modes occurring in vertical wellbore sub-aligned to one principal stress direction as shown in Fig. 3. A1 and A2 rupture modes correspond to the common wellbore breakouts with the tangential stress at the wellbore exceeding the strength of the rock. B1 and B2 modes result from excessive vertical stress relatively to the internal pressure. Excessive internal pressure relatively to external stress causes the C1 and C2 rupture modes that are believed to form due to elastic deformation in the unruptured parts of the wellbore, without producing cavings.

Focusing on A1, B1 and C1 rupture modes and based on the state of the drilling stresses responsible for each rupture mode, it is possible to establish the initial in-situ stress state and maximum mud weight for each case. Using Anderson's classification (Anderson, 1905), mode A1 is the result of thrusting stress regime while B1 and C1 are the result of an extensional stress regime. The values of the total principal stresses are summarised in Table 2.

Table 2. Principal stress magnitudes and stress ratio values for A1, B1, C1 rupture modes

	A1	**B1**	**C1**
Vertical stress, σ_v (psi)	*isotropic and anisotropic*		
	10195.7	12744.8	12744.8
Max horizontal stress, σ_H (psi) – *aligned N-S*	*isotropic and anisotropic*		
	12744.8	10195.7	10195.7
Min horizontal stress, σ_h (psi)	*isotropic*		
	12744.8	10195.7	10195.7
	anisotropic		
	11744.8	9800.7	9800.7
In-situ Pore Pressure, P_{form} (psi)	8131.09	8131.09	8131.09
Max mud weight, P_{mud} (psi)	9000	9000	12000

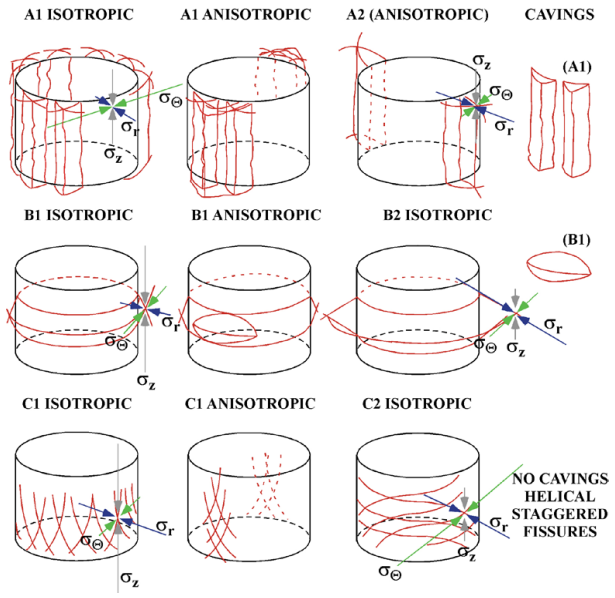

Fig. 3. Shear rupture modes around a vertical wellbore (after Etchecopar et al. (1999)).

The subsequent analyses accounting for planes of weakness and deviated wells are performed under the stress state of the first configuration, A1.

2.4. *Loading*

Loading of the wellbore includes the increase of the mud pressure during the excavation of the well, a period of constant pressure higher than the formation pressure (overbalance) and a subsequent decrease of the pressure to the formation pressure value. The loading curves for each case considered are shown in Fig. 4. The sensitivity

studies considering a heterogeneous host rock strength and an inclined well are subjected to the same loading as A1.

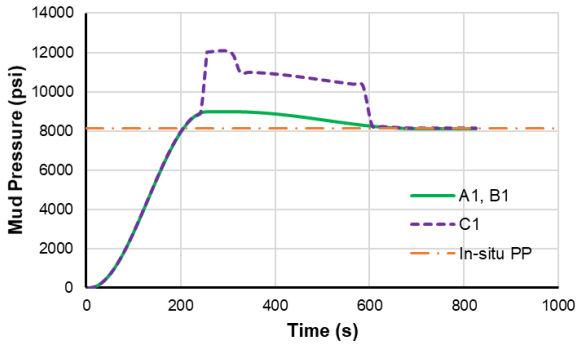

Fig. 4. Mud pressure vs time for cases A1, B1, C1.

3. RESULTS

3.1. Vertical well in isotropic formation

Using the Elfen wellbore software, six different configurations were investigated considering a vertical well aligned with the principal stress directions and in a homogeneous formation. The results for the first three cases that assume isotropy of the horizontal stresses are summarised in Fig. 5. The first column in Fig. 5 shows a horizontal section of the effective plastic strain around the wellbore right after the excavation of the well. The second column shows a horizontal section of the plastic strain at ~580 s, with the mud pressure being still higher than the formation pressure (see Fig. 4). The third column illustrates a vertical section of the well at ~580 s and the second line for each case shows the wellbore surface for 0-to-360° angle around the wellbore. The analyses described in sections 3.1.1 and 3.1.2 serve as a validation exercise before considering more complex scenarios not easily predicted analytically.

3.1.1. Isotropic stress field

Based on the rupture modes illustrated in Fig. 3, it is shown that all three failure patterns are well reproduced in our model. A1 configuration considers a thrusting stress regime and results to the well-known breakouts (Fig. 5b). The drilling stresses correspond to a maximum tangential stress, an intermediate vertical stress and a minimum radial stress. The breakouts occur all around the surface of the well as the in-situ horizontal stresses are identical and hence the resulting hoop stress does not vary as a function of the angle. The cavings are developing parallel to the well axis (vertically) as shown in Fig. 5c. Under a constant tangential stress and for a homogeneous formation, rupture is uniform around the wellbore.

For B1 configuration, the stress regime is extensional with the in-situ vertical stress being the highest while the loading of the well remains the same as in A1. The vertical stress is now the maximum stress, the tangential stress intermediate and the radial stress minimum. At 580 s, the horizontal section of the plastic strain shown in Fig. 5f appears different to the pattern observed in configuration A1 and is better visualised in Fig. 5g. The cavings in this case are the result of the high vertical stress applied on the well and are mainly developing in a perpendicular direction to the well axis.

C1 configuration assumes the same in-situ stress field as B1 but with a higher mud weight. Consequently, the order of the drilling stresses is slightly changed, with the vertical stress being still the highest, the radial being the intermediate due to the elevated mud weight and the tangential being the minimum. Under these conditions, no cavings are formed, instead, the rupture mode consists of helical shear fractures as illustrated in Fig. 5l. These fractures appear only on the surface of the well and do not produce any deteriorated material volumes like rupture modes A1 and B1. However, well fluid loss could be expected and induced fractures could propagate.

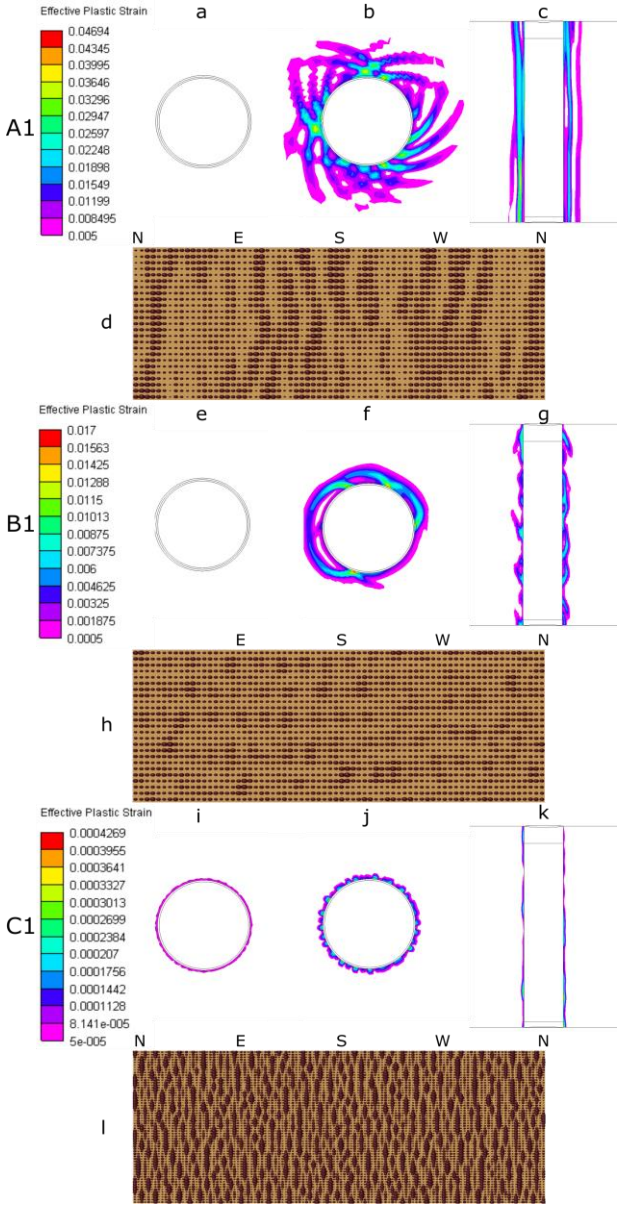

Fig. 5. Effective plastic for A1 isotropic stress field: (a) horizontal view at 255 s, (b) horizontal view at 580 s, (c) vertical view at 580 s, (d) wellbore surface at 580 s; B1 isotropic stress field: (e) horizontal view at 255 s, (f) horizontal view at 580 s, (g) vertical view at 580 s, (h) wellbore surface at 580 s; C1 isotropic stress field: (i) horizontal view at 255 s, (j) horizontal view at 580 s, (k) vertical view at 580 s, (l) wellbore surface at 580 s.

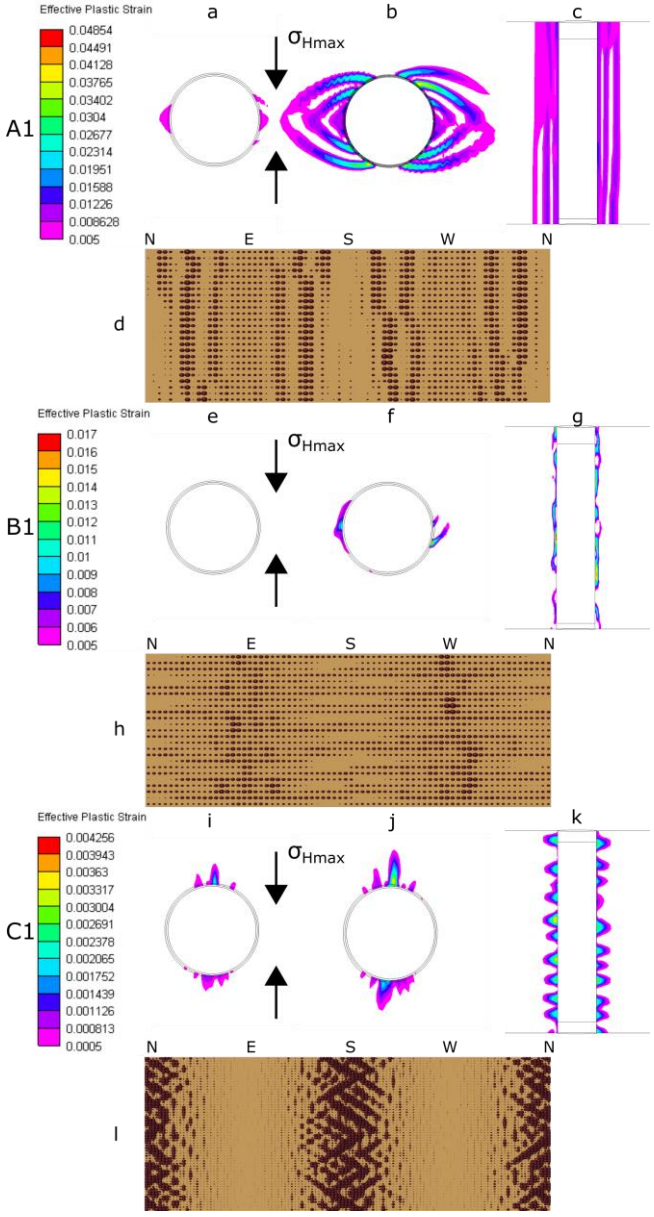

Fig. 6. Effective plastic for A1 anisotropic stress field: (a) horizontal view at 255 s, (b) horizontal view at 580 s, (c) vertical view at 580 s, (d) wellbore surface at 580 s; B1 anisotropic stress field: (e) horizontal view at 255 s, (f) horizontal view at 580 s, (g) vertical view at 580 s, (h) wellbore surface at 580 s; C1 anisotropic stress field: (i) horizontal view at 255 s, (j) horizontal view at 580 s, (k) vertical view at 580 s, (l) wellbore surface at 580 s.

3.1.2. Anisotropic stress field

The same rupture modes are investigated in this subsection for a vertical wellbore under an anisotropic state of the horizontal stresses (see Table 2).

In the cases A1, B1, C1 described here, the state of the drilling stresses is similar to the corresponding cases of the previous section. The only difference being the stresses varying as a function of angle around the wellbore due to the difference in the magnitude of the horizontal stresses. This difference results in a rather localised rupture mode along a favourable direction around the wellbore. Depending on the stress conditions, and mud pressure, the maximum stress can be either compressive or tensile. For a breakout type of failure (A1, B1), the cavings will appear on the wellbore sides

parallel to the maximum in-situ stress (E-W) where the tangential stress is expected to be a maximum. For the rupture mode observed in C1, the fractures will develop on the wellbore sides parallel to the minimum in-situ stress (N-S) where the tangential stress is expected to be a minimum.

Indeed, for A1 configuration (Fig. 6a, b, c, d), the breakouts are located in the E-W direction as shown in Fig. 6d, similarly for B1 (Fig. 6e, f, g, h). To reproduce the rupture mode observed in C1, the mud weight was increased by ~3,000 psi compared to the previous cases. For a high mud pressure, the wellbore is expected to fail in tension at the location of the maximum tensile stress (direction N-S). It can be seen in Fig. 6i, j, k that small fractures are developing as a result of the increased mud weight applied. However, because of the large difference between the vertical (σ_1) and minimum horizontal stress (σ_3), these fractures initiate as shear fractures on the surface of the well as shown in Fig. 5l.

During the simulation for the cases presented above, it was possible to calculate the continuously changing stresses around the wellbore and capture the post-yield behaviour of the material. It was therefore possible to track and calculate the volume of the elements around the wellbore initially yielding and subsequently experiencing strain softening. As the wellbore surface becomes damaged a criterion is used to determine the elements that no longer support high stresses and their volumes are calculated. This corresponds to both the deteriorated material around the wellbore and also undamaged cavings that are 'separated' from the wellbore surface; hence this calculation can provide an estimation of the additional expected cavings volume under specific conditions (in excess of the drilled wellbore). The criterion used for the calculation of the elements volume considers the elements characterised by an effective mean stress < 1000 psi. The evolution of the effective mean stress for the isotropic case A1 is shown in Fig. 7. The first three snapshots correspond to the different timings during the simulation: i) before drilling, ii) right after excavation, ii) during overbalance. The last snapshot of Fig. 7 shows the area around the wellbore with an effective stress < 1000 psi corresponding to the deteriorated and detached material volume.

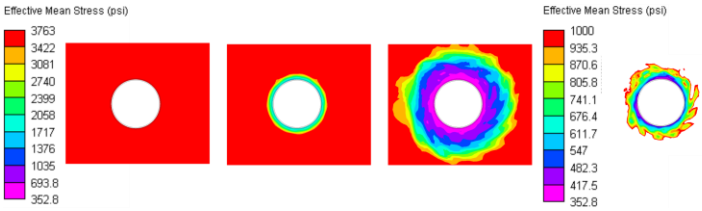

Fig. 7. Left: Evolution of the effective mean stress for the isotropic case A1 (t = 0, 255, 580 s). Right: Area around the wellbore characterised by an effective mean stress lower than 1000 psi.

Fig. 8 compares the effective mean stress at 580 s for all the theoretical rupture modes described above and Fig. 8 shows the evolution of the calculated volumes during the simulations.

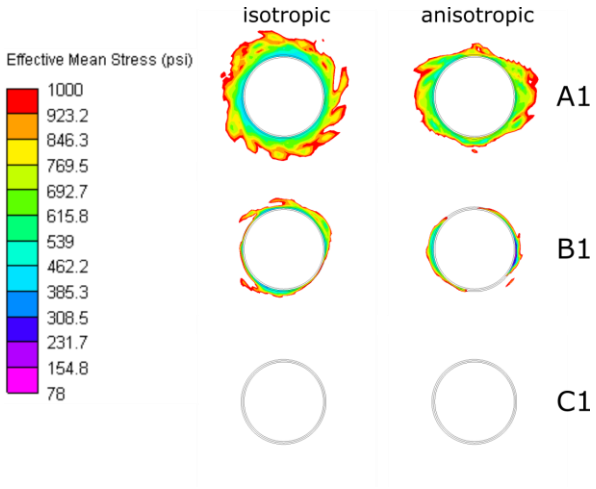

Fig. 8. Area around the wellbore characterised by an effective mean stress lower than 1000 psi for A1 isotropic, anisotropic stress field, B1 isotropic, anisotropic stress field, C1 isotropic, anisotropic stress field.

As expected, both Fig. 8 and Fig. 9 show that the largest volume of deteriorated material is produced for case A1 under an isotropic horizontal stress field. Generally, the development of cavings parallel to the well axis (vertically) leads to larger volumes of deteriorated material while the C1 rupture mode produces minimal amount of deteriorated material with most of the deformation taking place on the surface of the well.

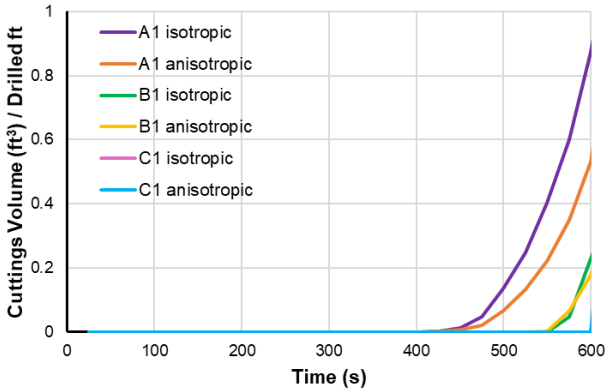

Fig. 9. Calculated total volume of elements per drilled foot with an effective mean stress < 1000 psi for A1, B1, C1 under isotropic and anisotropic stress field.

Quantitatively, considering case A1 at t = 580 s and for an isotropic horizontal stress field, it is possible to calculate the following:

$$V_{cuttings} = V_{well} + V_{breakout} = 0.491 + 0.601 = 1.09 \text{ ft}^3\text{/drilled foot}$$

where $V_{well} = \pi r^2 h/l$, is the wellbore volume per drilled foot, with r, h and l being the radius, height and length

of the wellbore respectively. $V_{breakout}$ is the volume of elements per drilled foot with an effective mean stress < 1000 psi

This estimation can be useful in providing information regarding the extent of damage around the well and the actual diameter of the well. Nevertheless, it should be noted that the results concerning predicted cutting volumes are presented to allow a direct comparison between the configurations considered and are not necessarily representative of in-situ conditions. In future work and based on this study, it is important that these values are validated and calibrated against real data coming from calipers or wellbore image logs.

The volumes calculated for each case shown in Fig. 9 can give an estimation of the dominant rupture mode depending on the in-situ conditions. The predicted cuttings volumes are summarised in Table 3.

Table 3. Predicted cuttings volume for A1, B1, C1 under isotropic and anisotropic stress field.

	Predicted $V_{cuttings}$ (ft^3/drilled ft)
A1 isotropic	1.09
A1 anisotropic	0.84
B1 isotropic	0.54
B1 anisotropic	0.56
C1 isotropic	0.49
C1 anisotropic	0.49

3.2. Vertical well in heterogeneous formation

Planes of weakness are introduced in the model to account for strength anisotropy of the formation. The in-situ conditions and mud pressure are the same as A1 anisotropic case (see Table 2). The least onerous case is considered initially where the vertical well is drilled perpendicularly to the planes of weakness (see Fig. 2a). This means that the angle of attack is 90°. Rotation of the well in a heterogeneous formation is described in Section 3.4.

The calculated effective plastic strain and effective mean stress for a vertical well drilled in a homogeneous and heterogeneous formation (PoW) are illustrated in Fig. 10.

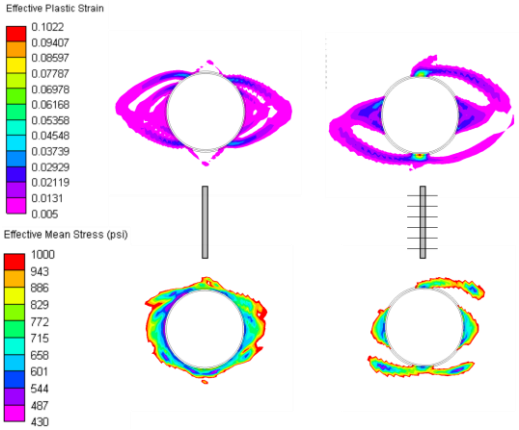

Fig. 10. Effective plastic strain and mean effective mean stress for well in homogeneous formation (left column) and well in heterogeneous formation (right column).

Compared to the homogeneous host rock case, when PoW are introduced in the model yielding occurs both in the minimum and maximum stress directions with higher but more localised deformation in the direction of the maximum stress. The observed plastic strain in this direction is associated with localised slip along the bedding planes. Keeping in mind, that the specific bedding orientation is not expected to cause serious problems during drilling as no significant amount of slip occurs, the volume of the cavings is lower than the homogeneous formation case (Fig. 11 and Table 4). This is the result of the difference in the elastic behaviour between the two cases. Deformation is accommodated by the "softer" planes of weakness in the normal and tangential direction, resulting in local stress reduction which does not significantly contribute to the volume calculation.

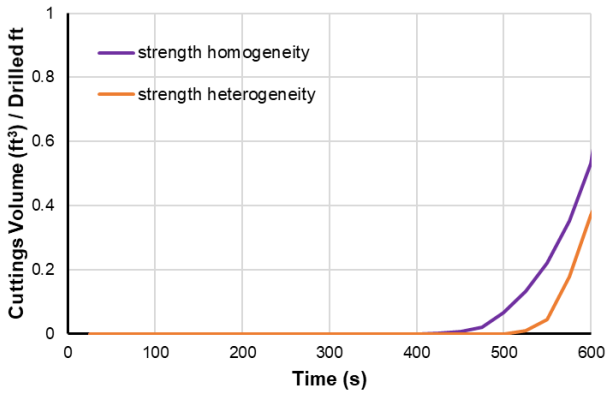

Fig. 11. Calculated total volume of elements per drilled foot with an effective mean stress < 1000 psi for well in homogeneous formation and well in heterogeneous formation.

Table 4. Predicted cuttings volume for well in homogeneous formation and well in heterogeneous formation.

	Predicted $V_{cuttings}$ (ft^3/drilled ft)
Strength homogeneity	0.84

Strength heterogeneity	0.67

3.3. Deviated well in heterogeneous formation

Under the same stress and pressure conditions as the A1 anisotropic case, the well is rotated by 30°, 60° and 90° (horizontal well) to assess wellbore stability and cavings volume for deviated wells in isotropic formations.

The orientation of the well, the failure mode and the effective mean stress are shown in Fig. 12. For a horizontal well orientation, the plastic strain appears to be limited compared to the other cases (Fig. 12, 90°) and develops in the direction of the minimum stress which is the vertical component in this configuration. For a 30˚ inclination well, the failure mode is similar to that developed around a vertical well, however affecting a larger volume of the formation. As the inclination increases to 60° yielding occurs all around the well offering complex patterns of plastic strain.

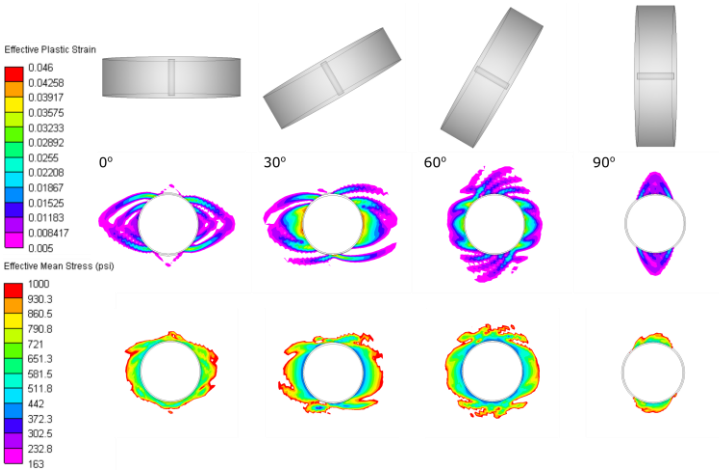

Fig. 12. Effective plastic strain (middle row) and mean effective mean stress (last row) for vertical well (1st column), 30° inclined well (2nd column), 60° inclined well (3rd column) and 90° inclined well (4th column).

The effective mean stress value around the wellbore follows the failure modes for each well orientation (Fig. 12 last row). Throughout the simulations, the largest volume of degraded material is observed for a well inclination of 30° (Fig. 13 and Table 5) due to the large extent of plastic strain around the well. For a well inclination of 60°, the affected volume is lower but appears to be more uniform around the well. The lowest volume is calculated for the horizontal well as for the same mud weight, the stresses acting on the plane of the well (σ_h, σ_v) are now lower in magnitude (σ_H acts in the axial direction of the well, see also Table 2).

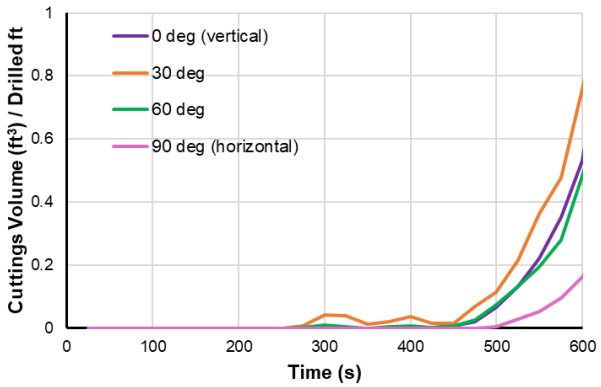

Fig. 13. Calculated total volume of elements per drilled foot with an effective mean stress lower than 1000 psi for vertical well, 30° inclined well, 60° inclined well and 90° inclined well.

Table 5. Predicted cuttings volume for vertical well, 30° inclined well, 60° inclined well and 90° inclined well.

Well inclination	Predicted $V_{cuttings}$ (ft^3/drilled ft)
0°	0.84
30°	0.97
60°	0.77
90°	0.59

3.4. Deviated well in heterogeneous formation

In this final section, the well is inclined by 0°, 30°, 60° and 90° into a heterogeneous formation. Considering horizontal bedding planes, these well inclinations correspond to angles of attack of 90°, 60°, 30° and 0° (see Fig. 2).

Fig. 14 shows qualitatively the area around the wellbore where bedding plane slip has occurred (2nd line), the effective plastic strain (3rd line) and effective mean stress (4th line) calculated during the simulations for each case.

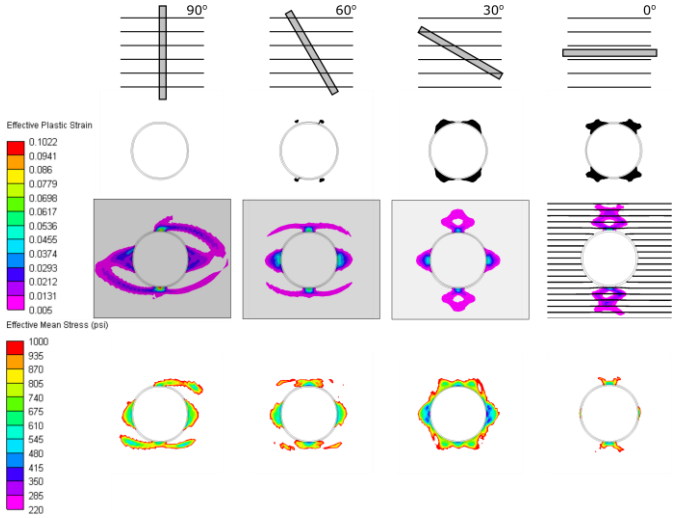

Fig. 14. Bedding slip (2nd row), effective plastic strain (3rd row) and mean effective mean stress (4th row) for attack angle of 90° (1st column), 60° (2nd column), 30° (3rd column) and 0° (4th column).

In terms of planes of weakness slip, for the 90° attack angle there is almost no slip along the bedding planes as this is considered the safest combination of well and beddings orientation (Okland and Cook, 1998). However, as the well is inclined it is obvious that the area affected by bedding slip becomes larger. These areas correspond to the locations where the stress conditions encourage the most bedding plane slip. The transition of the plastic strain location and pattern is also obvious as the well is rotated. For an attack angle of 0°, the failure mode observed is described in Section 3.2. For 30° attack angle, plastic strain associated to the host rock breakouts and the strain in the direction of the maximum stress (bedding slip) appears more limited (Fig. 14, 2nd column) as the angle of attack is slightly increased. For lower angles of attack ($0° < \theta < 30°$), the dominant failure mechanism is slip along the planes with the well-known buckling of the planes of weakness and subsequent fracturing extending in the direction normal to the planes of weakness. This mechanism results in the plastic strain pattern clearly shown in Fig. 14, for 0° attack angle (4th column).

As shown by the effective mean stress calculation (Fig. 14, 4th row), the configuration with the largest area affected is the one assuming an attack angle of 60° (see also Fig. 15 and Table 6). Nevertheless, it is comparable to the volumes calculated for the cases of attack angle of 90° and 60°. It is expected that for an angle of attack equal to 90°, the volume of degraded material is going to be lower (Fig. 15 and Table 6) as the dominant mechanism is bedding slip that does not cause significant changes in volume (apart from minor dilation in the plane). Therefore, the expected change of the effective mean stress in the model is minimal as shown in Fig. 14, for 0° case.

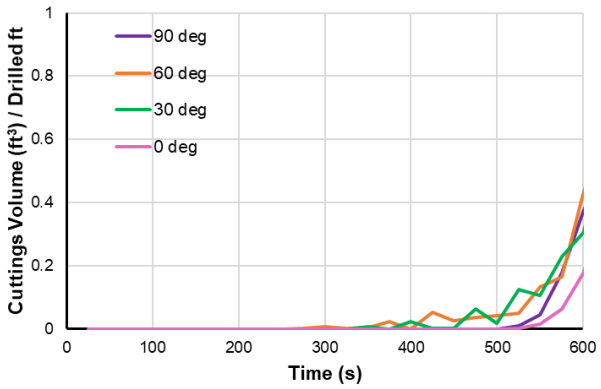

Fig. 15. Calculated total volume of elements per drilled foot with an effective mean stress lower than 1000 psi for attack angle of 90°, 60°, 30° and 0°.

Table 6. Predicted cuttings volume for attack angle of 90°, 60°, 30° and 0°.

Attack angle	Predicted $V_{cuttings}$ (ft^3/drilled ft)
90°	0.67
60°	0.65
30°	0.72
0°	0.56

4. CONCLUSIONS

Wellbore instability can pose serious problems in the drilling industry affecting many applications such as hydrocarbon recovery, CO_2 storage and enhanced geothermal systems amongst others. Numerical modelling consists of a robust tool for predicting instability issues that can arise under unfavourable in-situ conditions which are hard to assess analytically. In this study we use the Elfen wellbore software to investigate complex failure modes occurring when drilling in challenging environments. After validating the software against theoretical rupture modes, a sensitivity study was presented where the well alignment was varied with respect to the principal stress directions, drilled in a heterogeneous formation characterised by the presence of planes of weakness and a combination of both the above. The failure patterns observed for the configurations investigated were presented for a given interval of the wellbore considering uniform materials and stress conditions. As an extension to this study, it would be interesting to vary the rock properties along the wellbore length and assess the possible difference in the failure modes.

Making use of the software capabilities, it is possible to capture not only the failure patterns but also the post-yield softening response of the material and thus the dynamically changing stresses around the wellbore. With this information, we are able to calculate a

representative volume corresponding to both the deteriorated material around the wellbore and also undamaged cavings that are separated from the wellbore surface. This can provide useful estimations of the cuttings volume during drilling informing on the extent of instability. The combination of such modelling, results assessment techniques and real-time field monitoring can significantly limit the risks associated with drilling in increasingly difficult conditions.

REFERENCES

1. Altman, S.J., B. Aminzadeh, M.T. Balhoff, P.C. Bennett, S.L. Bryant, M.B. Cardenas, K. Chaudhary, R.T. Cygan, W. Deng, T. Dewers, D.A. DiCarlo, P. Eichhubl, M.A. Hesse, C. Huh, E.N. Matteo, Y. Mehmani, C.M. Tenney, and H. Yoon, 2014. Chemical and hydrodynamic mechanisms for long-term geological carbon storage. *J. Phys. Chem.* 118: 15,103–15,113.
2. Anderson, E. M. (1905). The dynamics of faulting. *Transactions of the Edinburgh Geological Society*, *8*(3), 387-402.
3. Ask, D., & Ask, M. V. S. (2006). Detection of potential borehole breakouts in boreholes KFM01A and KFM01B. *SKB P-report in prep.*
4. Bonnelye, A., Schubnel, A., David, C., Henry, P., Guglielmi, Y., Gout, C., ... & Dick, P. (2017). Strength anisotropy of shales deformed under uppermost crustal conditions. *Journal of Geophysical Research: Solid Earth*, *122*(1), 110-129.
5. Chen, S. L., & Abousleiman, Y. N. (2017). Wellbore stability analysis using strain hardening and/or softening plasticity models. *International Journal of Rock Mechanics and Mining Sciences*, *93*, 260-268.
6. Chen, S. L., Abousleiman, Y. N., & Muraleetharan, K. K. (2012). Closed-form elastoplastic solution for the wellbore problem in strain hardening/softening rock formations. *International Journal of Geomechanics*, *12*(4), 494-507.
7. Etchecopar, A., P. A. Pezard, and V. Maury. "New borehole imagery techniques: an aid for failure modes and in situ stress analysis and for minimizing drilling incidents." *SPWLA 40th Annual Logging Symposium*. Society of Petrophysicists and Well-Log Analysts, 1999.
8. Gaede, O., Karrech, A., & Regenauer-Lieb, K. (2013). Anisotropic damage mechanics as a novel approach to improve pre-and post-failure borehole stability analysis. *Geophysical Journal International*, 193(3), 1095-1109.
9. Ghassemi, A., 2012. A review of some rock mechanics issues in geothermal reservoir development. *Geotech. Geol. Eng*. 30: 647–664.
10. Konstantinovskaya, E., Laskin, P., Eremeev, D., Pashkov, A., Semkin, A., Karpfinger, F., ... & Trubienko, O. (2016, October). Shale Stability When Drilling Deviated Wells: Geomechanical Modeling of Bedding Plane Weakness, Field X, Russian Platform (Russian). In *SPE Russian Petroleum Technology Conference and Exhibition*. Society of Petroleum Engineers.
11. Labiouse, V., & Vietor, T. (2014). Laboratory and in situ simulation tests of the excavation damaged zone around galleries in Opalinus Clay. *Rock Mechanics and Rock Engineering*, *47*(1), 57-70.
12. Lang, J., Li, S., & Zhang, J. (2011, January). Wellbore stability modeling and real-time surveillance for deepwater drilling to weak bedding planes and depleted reservoirs. *In SPE/IADC Drilling Conference and Exhibition.* Society of Petroleum Engineers.
13. Mehrabian, A., Pérez, A. D., & Santana, C. (2018). Wellbore-stability analysis considering the weak bedding planes effect: a case study. *SPE Drilling & Completion*, *33*(04), 377-384.
14. Moeck, I., and T. Backers, 2011. Fault reactivation potential as a critical factor during reservoir stimulation. *First Break* 29: 73–80.
15. Okland, D., & Cook, J. M. (1998, January). Bedding-related borehole instability in high-angle wells. In *SPE/ISRM rock mechanics in petroleum engineering*. Society of Petroleum Engineers.
16. Ong, S. H., & Roegiers, J. C. (1993, December). Influence of anisotropies in borehole stability. In *International Journal of Rock Mechanics and Mining Sciences & Geomechanics Abstracts* (Vol. 30, No. 7, pp. 1069-1075). Pergamon.
17. Rutqvist, J. (2012). The geomechanics of CO 2 storage in deep sedimentary formations. *Geotechnical and Geological Engineering*, *30*(3), 525-551.
18. Schultz, R. A., Mutlu, U., & Bere, A. (2016, June). Critical issues in subsurface integrity. In *Paper ARMA 16-037 presented at the 50th US Rock Mechanics/Geomechanics Symposium* (Vol. 26, p. 29).
19. Streit, J.E., and R.R. Hillis, 2004. Estimating fault stability and sustainable fluid pressures for underground storage of CO_2 in porous rock. *Energy* 29: 1445–1456.
20. Tellez, C. P., Alcantara Contreras, L., Cabrera, J. R., & Balasejus, D. (2012, January). Pre-Drill WBS Evaluation: Plane of Weakness and Well Design-A Case Study in the South of Mexico. *In IADC/SPE Asia Pacific Drilling Technology Conference and Exhibition.* Society of Petroleum Engineers.
21. Willson, S. M., Edwards, S. T., Crook, A. J., Bere, A., Moos, D., Peska, P., & Last, N. C. (2007, January). Assuring stability in extended reach wells-analyses, practices and mitigations. *In SPE/IADC Drilling Conference.* Society of Petroleum Engineers.
22. Willson, S. M., Last, N. C., Zoback, M. D., & Moos, D. (1999, January). Drilling in South America: a wellbore stability approach for complex geologic conditions. In

Latin American and Caribbean petroleum engineering conference. Society of Petroleum Engineers.

23. Zhang, J. (2013). Borehole stability analysis accounting for anisotropies in drilling to weak bedding planes. *International journal of rock mechanics and mining sciences, 60*, 160-170.

24. Zhou, J., He, S., Tang, M., Huang, Z., Chen, Y., Chi, J., ... & Yuan, P. (2018). Analysis of wellbore stability considering the effects of bedding planes and anisotropic seepage during drilling horizontal wells in the laminated formation. *Journal of Petroleum Science and Engineering*, *170*, 507-524.

25. Zoback, M. D. (2010). *Reservoir geomechanics.* Cambridge University Press.

26. Zoback, M.D., and S.M. Gorelick, 2012. Earthquake triggering and large-scale geologic storage of carbon dioxide. *Proc. US Nat. Acad. Sci*. 109: 10,164–10,168.